



# Hybrid chain reaction nanoscaffold-based functional nucleic acid nanomaterial cascaded with rolling circle amplification for signal enhanced miRNA let-7a detection

Hao Jiang<sup>1</sup> · Zhao Peng<sup>1</sup> · Xuefei Lv<sup>1</sup> · Ying Liu<sup>1</sup> · Xiaoqiong Li<sup>1</sup> · Yulin Deng<sup>1</sup>

Received: 2 May 2024 / Accepted: 30 July 2024 / Published online: 13 August 2024  
© The Author(s), under exclusive licence to Springer-Verlag GmbH Austria, part of Springer Nature 2024

## Abstract

A novel functional nucleic acid (FNA) nanomaterial based on hybrid chain reaction (HCR) nanoscaffolds is proposed to solve the problem of time superposition and repeated primer design in sensitive miRNA detection using cascade amplification technique. Rolling circle amplification (RCA) was cascaded with the prepared FNA nanomaterials for miRNA let-7a (as a model target) sensitive detection by lateral flow assay (LFA). Under the optimal conditions, the proposed RCA-FNA-LFA assay demonstrated the specificity and accuracy for miRNA let-7a detection with a detection limit of 1.07 pM, which increased sensitivity by nearly 20 times compared with that of RCA-LFA assay. It is worth noting that the non-target-dependent self-assembly process of HCR nanoscaffolds does not take up the whole detection time, thus, less time is taken than that of the conventional cascaded method. Moreover, the proposed assay does not need to consider the system compatibility between two kinds of isothermal amplification techniques. As for detection of different miRNAs, only the homologous arm of the padlock probe of RCA needs to be changed, while the FNA nanomaterial does not need any change, which greatly simplifies the primer design of the cascaded amplification techniques. With further development, the proposed RCA-FNA-LFA assay might achieve more sensitive and faster results to better satisfy the requirements of clinical diagnosis combining with more sensitive labels or small strip reader.

**Keywords** Functional nucleic acid · Nanoscaffold · Hybrid chain reaction · Rolling circle amplification · Lateral flow assay · MiRNA let 7a · Cascaded amplification

## Introduction

Isothermal amplification technique is one of the hot research topics in the field of rapid and sensitive nucleic acid (NA) detection [1]. However, different isothermal amplification methods have their own limitations, such as the low efficiency of rolling circle amplification (RCA) for long sequence NA detection, the difficulty of loop-mediated isothermal amplification (LAMP) primer design for short sequence NA detection, and the poor amplification ability of enzyme-free

isothermal amplification techniques for NA detection [2, 3]. Cascaded amplification technique is the integration of several nucleic acid isothermal amplification, with the output of the first layer amplification as the input of the next layer [4]. Cascaded amplification techniques, by integrating the characteristic of different isothermal amplification techniques, shows a great advantage in rapid and sensitive detection of NA, especially for trace NA detection [5].

At present, there are still two obvious problems with cascaded amplification [6]. One is that the mainstream cascaded amplification is carried out sequentially, that is, when the first layer of amplification is completed, the second stage of amplification is triggered. The amplification process is therefore more time-consuming. Although some cascades of one-pot method have been carried out, the optimal conditions for different isothermal amplification are not completely consistent, which makes it difficult for one-pot method to obtain an optimal condition suitable for multiple reaction systems [7]. Therefore, the sensitivity of

---

Hao Jiang and Zhao Peng contributed equally to this work.

✉ Xuefei Lv  
xuefeilv@163.com

<sup>1</sup> Beijing Key Laboratory for Separation and Analysis in Biomedicine and Pharmaceuticals, School of Medical Technology, Beijing Institute of Technology, Beijing 100081, China

the cascaded amplification is sacrificed to a certain extent. Different from polymerase chain reaction (PCR), which has a special primer-assisted design software, primer design of isothermal amplification technique lacks a perfect design mechanism [8]. Therefore, primer screening is an important and complex work. In cascaded amplification, the primer design of the second layer is usually dependent on the primers or the products of the first layer, which leads to different targets or even the same target using different primers [9–11]. It not only increases redundant work but also inevitably causes the waste of resources [12]. Therefore, a new idea of cascaded amplification is needed to be put forward to realize the efficient and sensitive nucleic acid detection, while the complexity of primer design and reaction time was reduced.

Functional nucleic acids (FNAs) are a class of non-genetic nucleic acids and their analogues that have a special structure and perform a specific biological function [13–15], including aptamers, DNazymes, ribose switches, G-quadruplex, and etc. As a powerful biomolecule, FNAs have shown unique charm in the fields of biosensing, bioimaging, material assembly, targeted delivery, and disease therapy [16, 17]. Meanwhile, study on the assembly of FNAs with nanomaterials have been carried out, because of the well-arranged hydrophobic/hydrophilic and easily modified functional groups, flexible structures, high efficiency catalytic capacity, and the potential of constructing complex structures and patterns of various FNAs [18].

Inspired by these researches, a FNA nanomaterial based on HCR nanoscaffold and probe hybridization was proposed in the present study to solve two important problems in cascaded amplification, that is, amplification time-consuming and probe repeated design. In the proposed cascaded amplification, RCA was used as first-layer amplification, and HCR-based functional nucleic acid nanomaterials mediated secondary-layer amplification. This self-assembly process of the HCR-based FNA nanomaterial was independent of the target sequence. Hence, it can be performed before the cascade amplification, which didn't occupy the total amplification time. As a result, the full time for the miRNA detection was only 2 h. In addition, the proposed method can be used for amplify different targets only by simply changing the homologous arm sequence of the padlock probe without the limitation of probe sequence dependence. As a proof-of-concept experiment, miRNA let-7a, involved in tumor suppression [19, 20], was chosen as a model biomarker for cascaded amplification and LFA detection. Compared with previous studies, the sensitivity of proposed cascade amplification technique based on RCA and self-assembly FNA nanomaterial coupled with lateral flow assay (RCA-FNA-LFA) was enhanced nearly 20 times than that of RCA-LFA without reaction time increasing. Meanwhile, different from other cascaded amplification methods, the detection

time of the proposed RCA-FNA-LFA depends only on the time consumed by the first layer amplification of RCA, which will help speed up the whole detection process. At the same time, standardized FNA probe design methods will reduce the repetitive work and improve the detection efficiency.

## Materials and methods

### Reagents and materials

Nucleic acid (Table 1), fetal bovine serum (FBS), Triton-X-100, and Tween-20 were purchased from Sangon Biotech (Shanghai, China). Splint R Ligase, phi29 DNA polymerase, and Nb.BbvCI were purchased from New England Biolabs (Beijing, China). Bovine serum albumin (BSA), streptavidin (SA), phosphate buffered saline (PBS), and Tris-EDTA (TE) buffer were purchased from Beijing solarbio science & technology (Beijing, China). Nitrocellulose (NC) membrane and Amicon Ultra-0.5 centrifugal filter unit with Ultracel-30 membrane were purchased from Merck Millipore (Darmstadt, Germany). Glass fibers, polystyrene, and polyvinyl chloride backing pad, and absorbent papers were purchased from Jiening Biotech (Shanghai, China). All other chemical reagents used in the experiment were obtained from Sinopharm Chemical Reagent Co., Ltd. (Beijing, China). All water for solution preparation was obtained from the MilliQ Water Purification System of Merck Millipore (Darmstadt, Germany).

### The self-assembly of HCR nanoscaffold-based FNA nanomaterial

#### Design and analysis of hairpin probes

According to the principle of HCR [21–23], the corresponding hairpin probes were designed for the given initiator probe (IP). Sequences of hairpin probes were analyzed by NUPACK (<http://www.nupack.org/>), which was defined in 0.75 M Na<sup>+</sup> as a testing benchmark.

#### Characterization of HCR nanoscaffold

100  $\mu$ L SPSC buffer containing H1F (1  $\mu$ M) and H2F (1  $\mu$ M) were reacted with 0.3  $\mu$ M IP at 37°C for 12 h, and then the amplified product was centrifuged at 12,000 rpm for 15 min and replenished the solution to be 25  $\mu$ L. The self-assembly products were characterized by 2% agarose gel electrophoresis and were observed under the Gel Doc-XR Imaging System (Biorad, USA).

**Table 1** Nucleic sequences used in this study

Probe	Target sequence (5'–3')
ssDNA let-7a	TGAGGTAGTAGGTTGTATAGTT
miRNA let-7a	UGAGGUAGUAGGUUGUAAGUU
LP let-7a	P-CTGATAAGCTAAGTCTCCTACCCTCAGCCTCCTTCAACATCAGTCTGATAAGCTAAG TCTCCTACCCTCAGCCTCCTTCAACATCAGT
T line let-7a	AACTATACAACCTACT-Biotin
C line let-7a	Biotin- AAAAAA GAGGGTAGGAGACT
H1	ATTTGGTTCCATTTTACCAGCTCAAAGTAGCTGGTAAAAATGGAA
H2	AGCTGGTAAAAATGGAACCAAATTTCCATTTTACCAGCTACTTTG
H1F	ATTTGG TTCCATTTTACCAGCT CAAAGTAGCTGGTAAAAATGGAA GGGGTGCCACCTCC
H2F	TGCCACCTCCGGGGAGCTGGTAAAAATGGAACCAAATTTCCATTTTACCAGCT ACTTTG
Initiator probe (IP)	AGCTGGTAAAAATGGAACCAAATAAAAAGTCTCCTACCCTCA
Tag probe	(CH <sub>2</sub> ) <sub>6</sub> -SH- AAAAAAAGGAGGTGGCA
miRNA let-7b	UGAGGUAGUAGGUUGUGUGUU
miRNA let-7c	UGAGGUAGUAGGUUGUAUGUU
miRNA let-7f	UGAGGUAGUAGUUGUAUAGUU
miRNA 202	AGAGGCAUAGGGCAUGGGAAAA
miRNA 98	CUAUACAACUACUACUUCCU
miRNA 21	UAGCUUAUCAGACUGAUGUUGA
miRNA 133	UUGGUCCCCUUAACCAGCUG

### Preparation and functionalization of AuNPs

AuNPs was synthesized according to the previously reported sodium citrate reduction method [24]. In short, 1 mL of chloroauric acid solution (1%, w/v) was added to 100 mL of ultrapure water, and the mixture was heated to the boiling. After about 2 min, the color of the solution changed and lasted for 5 min. When the color of the solution was stable, continuing to heat for 10 min. Then the solution was cooled to room temperature away from light, patching to be 100 mL. The prepared AuNPs was stored at 4°C away from light for later use.

In order to graft DNA tag probes onto the surface of AuNPs, 1 mL of AuNPs were firstly concentrated 4 times and the pH value was adjusted to be 8.0. At the same time, 200 µL of thiol-modified DNA tag probes (15 µM) were mixed with 5 µL of TCEP (1 M) and reacted for 30 min to activate the sulfhydryl group. Afterward, the prepared AuNPs and thiol-modified DNA probes were mixed and incubated at room temperature for 1 h. Then, 4.5 µL of sodium citrate solution (500 mM, pH 3) and NaCl (12 µL, 1 M) were added successively and was incubated at room temperature for 1 h. After that, 60 µL of HEPES (500 mM, pH 7.6) was added to adjust the solution to be weakly alkaline. Finally, the surface was blocked with 10% BSA and was incubated at room temperature for 2 h. The solution containing AuNPs@DNA complex was centrifuged at

12,000 rpm for 15 min and was washed three times with Tris-HCl (10 mM, pH 7.0) and was resuspended in 100 µL of Tris-HCl (10 mM, pH 7.0). The obtained AuNPs@DNA was stored at 4°C away from light for further use.

### Preparation of HCR nanoscaffold-based FNA nanomaterial

The obtained AuNPs@DNA solution was mixed with the prepared HCR nanoscaffold at the ratio of 1:1 (v/v), and was incubated at room temperature for 2 h. Then the HCR nanoscaffold-based FNA nanomaterial conjugate was obtained and was stored at 4°C away from light for further use.

### RCA reaction

The RCA reaction was operated using a 10 µL of reaction mixture containing 1.5 U Splint R ligase, 200 nM padlock probe (LP), 200 nM miRNA, 300 µM dNTPs, and 0.4 U Phi29 DNA polymerase. The reaction mixture was incubated at 37 °C for 2 h, then was denatured at 65 °C for 20 min, and finally was naturally cooled to room temperature. The RCA products were characterized by 2% agarose gel electrophoresis and were observed under the Gel Doc-XR Imaging System (Biorad, USA).

## RCA-FNA-LFA for miRNA let-7a detection

Prior to assembly, the sample pad was blocked with 10 mM PBS solution (0.1% Tween 20 v/v and 1% BSA w/v) for 30 min. The ssDNA probes of C line and T line, which reacted with 1 mg/mL streptavidin, were immobilized on the test line and control line by the BioDot XYZ platform (XYZ3010, Shanghai Kinbio Technology, Shanghai, China), respectively. The NC membrane with T line and C line was dried at 37 °C overnight. Finally, the NC membrane, sample pad, and absorbent pad were pasted on a PVC backing card successively. After assembly, it was cut into 4-mm and was stored at room temperature in a sealed bag.

100  $\mu$ L of reaction solution (5 $\times$ SSC) including sample, FNA nanomaterial, RCA products, and detergent (Triton X-100) were mixed in the ELISA well. Then, a test strip was inserted into this reaction solution at room temperature for 10 min. The reaction solution flowed through the NC membrane via capillary action. The bands of the T line and C line were photographed by a mobile phone and were analyzed by Image J software.

## Results and discussion

### Principle of HCR nanoscaffold-based self-assembly FNA nanomaterial

The FNA nanomaterial was self-assembled based on HCR nanoscaffold and the principle of Watson–Crick base pairing (Fig. 1). In the self-assembly process of HCR nanoscaffold, initiator probe (IP) acts as the initiator of HCR, opening the hairpin structure of H1F probe. The exposed sticky end of H1F probe can open the hairpin structure of H2F probe, as well as H2F probe and H1F probe open successively to form dsDNA. At the same time, AuNPs were modified with thiol-modified DNA tag probes by Au–S bond, and AuNPs@DNA was formed. A functional arm of H1F probe and H2F probe was designed to bind with AuNPs@DNA to complete the self-assembly of FNA nanomaterial and to obtain the HCR nanoscaffold-based FNA nanomaterial.

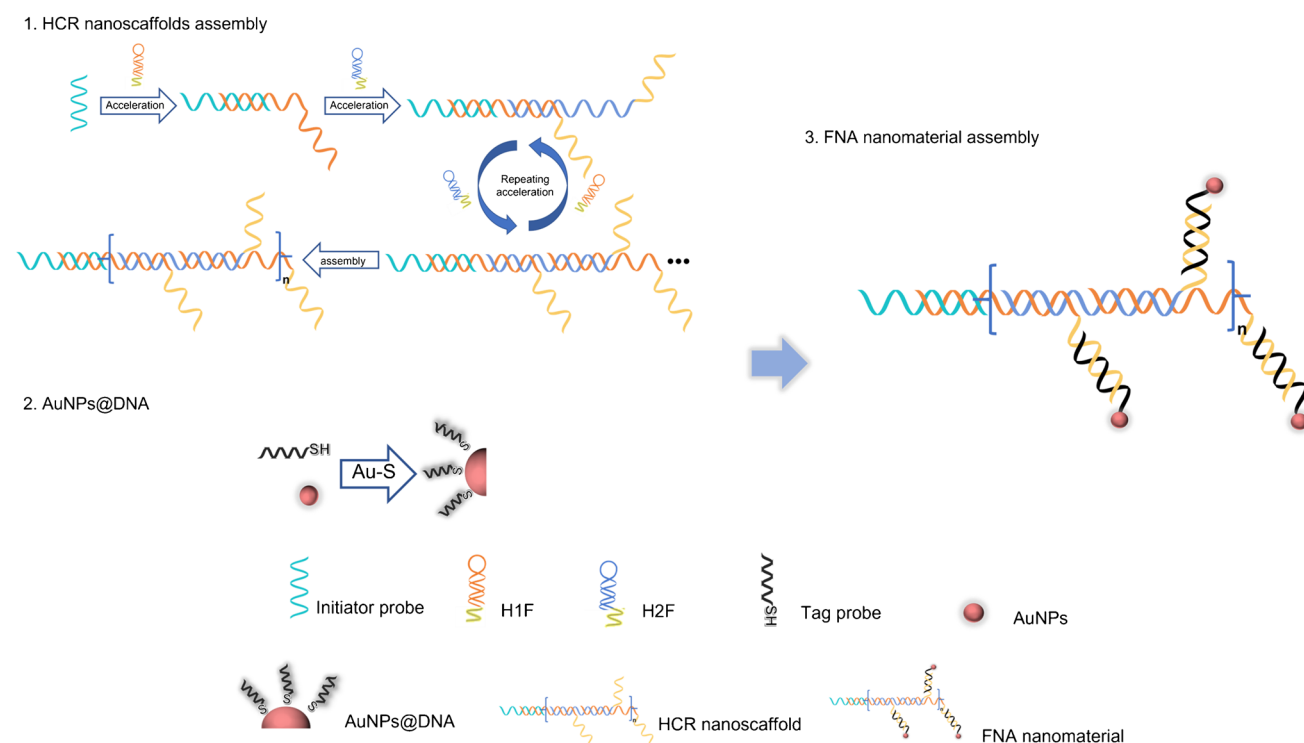


**Fig. 1** Principle of the self-assembly FNA nanomaterial

## Characterization and optimization of the self-assembly HCR nanoscaffolds

### Simulation and characterization of the self-assembly HCR nanoscaffolds

The reaction kinetics and product stability of the self-assembly HCR nanoscaffold were simulated by NUPACK (<https://nupack.org/>), a computer program developed by Harvard biophysicists Zachary Johnson and William Shih to predict the structure and stability of nucleic acid molecules, which has gradually evolved into a software platform containing multiple tools and algorithms [25, 26]. The initial concentration of H1F probe and H2F probe was set to be 1  $\mu\text{M}$ , while the initial concentration of IP probe was set to be 0.1  $\mu\text{M}$ , and the maximum complex product was set to be 5 components. As shown in Fig. 2A, at maximum reaction limits, all IP probes were used to initiate the HCR reaction (Column 3) without either by-products or leakage expression. The simulation of the product structure was shown in Fig. 2B, which showed the IP probe successfully initiated the self-assembly process and was bound with H1F probe and H2F probe at the terminal. The free energy changing of the last H2F probe terminal indicated its potential to be continued to bind with new probes. In addition, agarose gel electrophoresis was used to characterize the actual occurrence of the

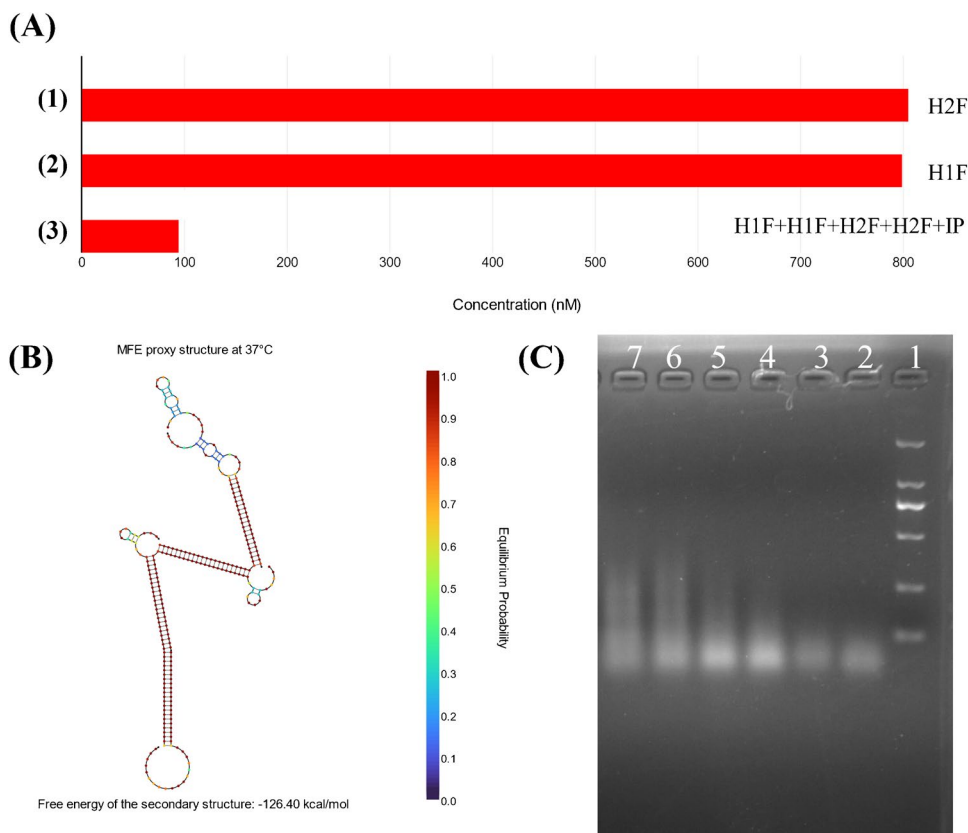
self-assembly. As shown in Fig. 2C, Lane 2 (H1F), Lane 3 (H2F), and Lane 4 (H1F and H2F) only have bands of low molecular weight, indicating that harpin probes could be stable in solution. Nevertheless, with the presence of IP probe, bands of high molecular weight with diffuse distribution appeared, indicating that HCR was successfully occurred, and the HCR nanoscaffold for the following experiment was successfully prepared.

### Optimization of the conditions for self-assembly HCR nanoscaffold

HCR was a chemical equilibrium reaction. The key to successfully construct HCR system was the design of harpin probe and terminal modification. It is not only necessary to ensure the efficient process of self-assembly, but also to avoid leakage expression in the absence of initiator. In particular, the bifunctional harpin probe designed in this study not only recognized the initiator to complete the capture of the amplified product, but also to combine with the AuNPs@DNA to realize the signal output.

The HCR reaction required the assistance of cations. However, high concentration of cations would reduce the stability of AuNPs@DNA complex. Thus, it was necessary to desalt the HCR products before coupling with AuNPs@DNA. This process was accomplished with the help of

**Fig. 2** Principle, design, and characterization of self-assembly FNA nanomaterial (A) Simulation of the self-assembly HCR nanoscaffold. (1) remaining H2F probe. (2) remaining H1F probe. (3) Principal product: IP + H1F + H2F + H1F + H2F. IP: 0.1  $\mu\text{M}$ . Other probes were 1  $\mu\text{M}$ . (B) Simulation of principal product for HCR nanoscaffold. (C) Characterization of the self-assembly HCR nanoscaffold. Lane 1: D2000 marker. Lane 2: H1F. Lane 3: H2F. Lane 4: H1F + H2F. Lane 5–7: IP + H1F + H2F. IP (5–7): 0.1, 0.3, 0.5  $\mu\text{M}$ . H1F with 1  $\mu\text{M}$  H2F, respectively



ultrafiltration tubes, which helped to concentrate the formed FNA products at the same time. After ultrafiltration, the dispersion band in Lane 2 was significantly brighter than that in Lane 3 (Fig. 3A), indicating that the HCR products were concentrated and the salts in the system were removed.

In addition, the reaction time of HCR was optimized. The conventional HCR reaction was fast which consumed 0.5 h to 2 h [27–29]. However, during this time period, the reaction did not reach its maximum. At the same time, as the functions of hairpin probe become more complex, the time consumed also increased [30–32]. The reaction volume of 100  $\mu\text{L}$  reaction buffer containing H1F probe and H2F probe (1  $\mu\text{M}$ ) with different IP probe concentration was carried out at room temperature for 6 h [Fig. 3B(a)], 12 h [Fig. 3B(b)], and 24 h [Fig. 3B(c)], respectively. As shown in Fig. 3B, in 12 h of HCR, the bands at the low molecular weight position became very light, the brightness of the bands at high molecular weight was significantly enhanced instead, which was obviously different from the reaction of 6 h and 24 h. Therefore, 12 h was chosen as the optimal reaction time for HCR. Meanwhile, comparing the results of lane 2–6 in 12 h

of HCR [Fig. 3B(b)], it can be found that with the increase of IP concentration (0.1–0.5  $\mu\text{M}$ ), the average molecular weight in the product decreased. In order to ensure that the HCR nanoscaffold can combine more AuNPs@DNA to provide a stronger signal, the probe ratio of lane 2 was selected, that was, IP: H1F: H2F = 1:10:10.

### Characterization of the prepared AuNPs@DNA

The UV absorption spectra was used to characterize the prepared AuNPs@DNA, and the result was shown in Fig. 4. It can be found from Fig. 4A that before coupling with DNA tag probe, the maximum absorption peak of AuNPs was located at 520 nm (solid red line), and after coupling with DNA tag probe, the absorption peak was changed to about 526 nm (solid green line), a redshift of the maximum absorption peak was occurred. At the same time, a distinct absorption peak appeared at 280 nm for AuNPs@DNA, which indicated that the diameter of AuNPs increased after coupling with DNA tag probe, the coupling between AuNPs and DNA tag probe was successful.

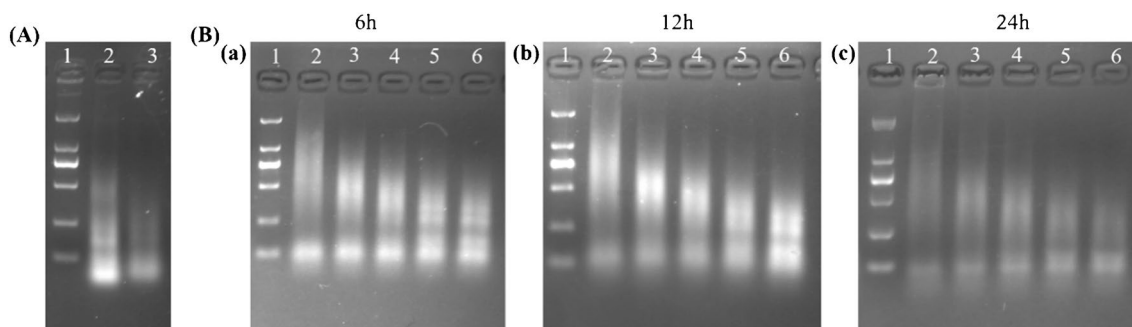


**Fig. 3** Optimization of FNA self-assembly based on HCR reaction (A) Concentration and desalting for self-assembly FNA. (B) Optimization self-assembly time for FNA. (a) FNA self-assembly for 6 h. Lane 1: D2000 marker. Lane 2–6: IP at the concentration of 0.1, 0.2,

0.3, 0.4, and 0.5  $\mu\text{M}$ . (b) FNA self-assembly for 12 h. Lane 1: D2000 marker. Lane 2–6: IP at the concentration of 0.1, 0.2, 0.3, 0.4, and 0.5  $\mu\text{M}$ . (c) FNA self-assembly for 24 h. Lane 1: D2000 marker. Lane 2–6: IP at the concentration of 0.1, 0.2, 0.3, 0.4, and 0.5  $\mu\text{M}$

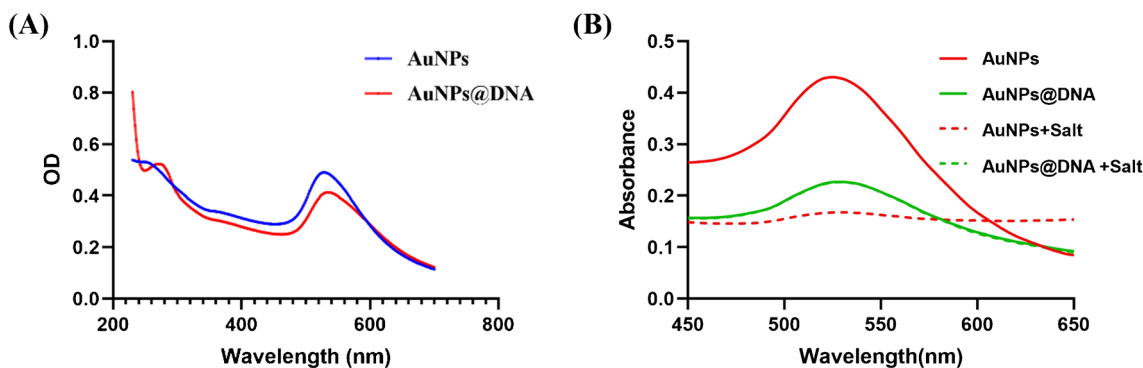


**Fig. 4** Characterization of AuNPs and AuNPs@DNA by UV absorption spectra (A). The UV absorption spectra of AuNPs and AuNPs@DNA. (B). The stability of AuNPs and AuNPs@DNA

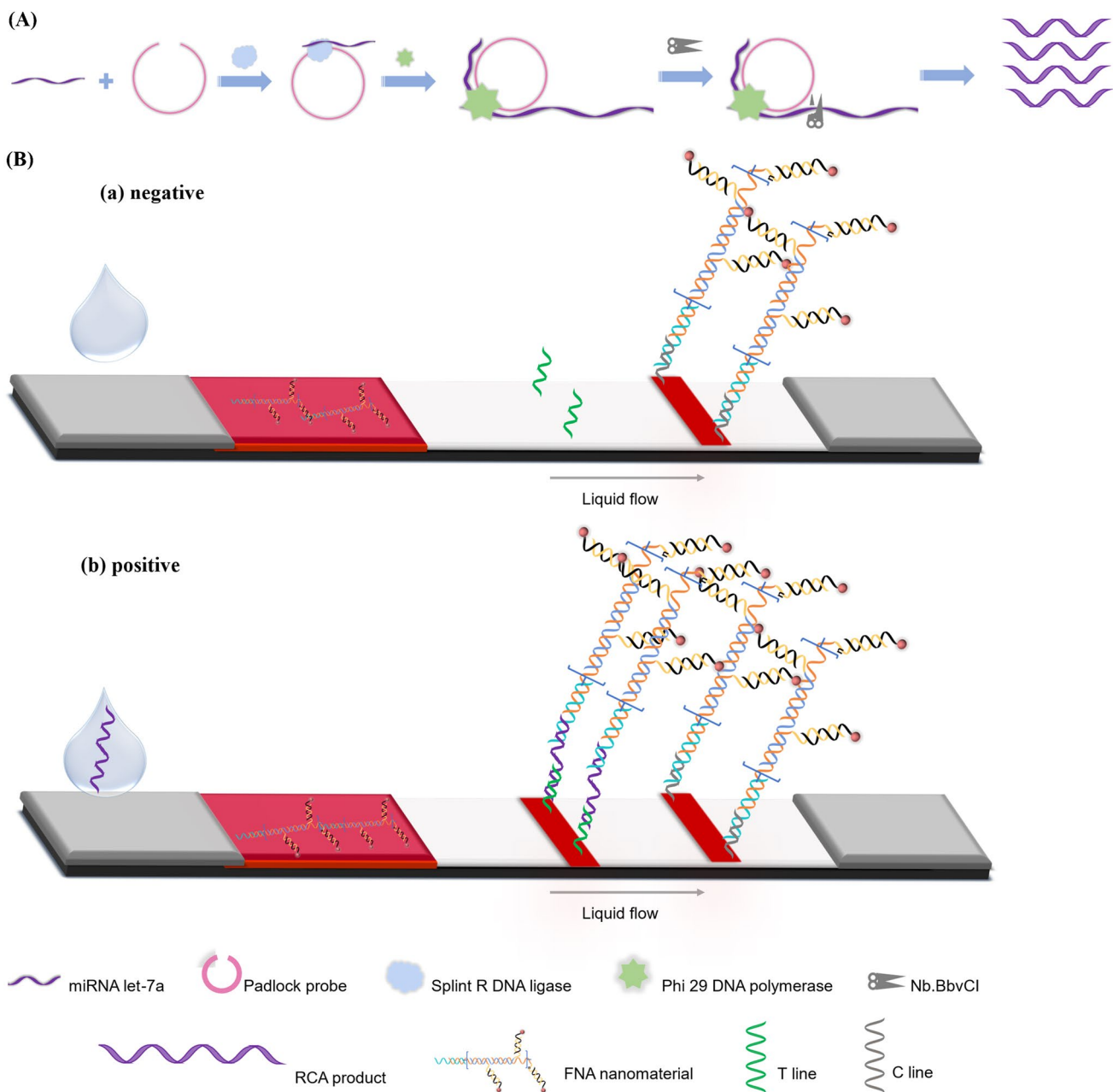


**Fig. 5** The principle of the proposed RCA-FNA-LFA assay for miRNA let-7a detection (A). The principle of RCA reaction. (B). The principle of RCA-FNA-LFA

In addition, Meys stabilization experiment was used to investigate the stability of the formed AuNPs@DNA (Fig. 4B). When excessive NaCl solution was mixed with AuNPs, the charge balance between AuNPs was destroyed by sodium ions, resulting in the aggregation of AuNPs, while the surface of AuNPs@DNA was coupled with nucleic acids, which could protect AuNPs from aggregation. After NaCl was added to the AuNPs solution, the changes were drastic of the UV absorption spectra (solid red line to dotted red line), while the UV absorption spectra of the AuNPs@DNA did not change much

before and after salt was added (dotted green line was overlapped with solid green line), which further proved that the DNA tag probe coupling with AuNPs was successful.

**HCR nanoscaffold-based FNA nanomaterial cascaded with RCA and coupled with lateral flow assay (RCA-FNA-LFA) for miRNA let-7a detection**

The principle of HCR nanoscaffold-based FNA nanomaterial cascaded with RCA and coupled with lateral flow assay

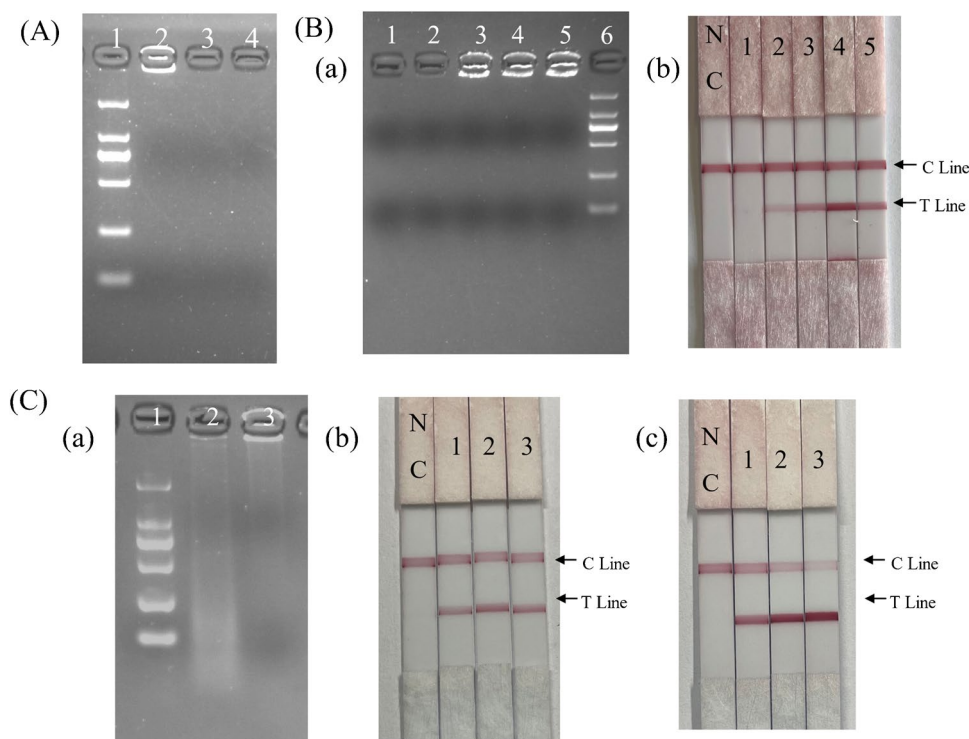


**Fig. 6** Optimization of RCA conditions for RCA-FNA-LFA assay (A). Specificity evaluation of padlock probe for RCA. Lane 1: D2000 marker. Lane 2: miRNA let-7a+padlock probe let7a. Lane 3: miRNA 21+padlock probe let7a. Lane 4: miRNA 211+padlock probe let7a. (B). Optimization of the padlock probe concentration for RCA. (a) The result of agarose gel electrophoresis. The concentration of padlock probe in lane 1–5 was 1, 5, 10, 50, 100 nM, respectively. (b) The result of LFA. The concentration of padlock probe in strips 1–5 was 1, 5, 10, 50, 100 nM, respectively. All miRNA concentrations used in the experiment was 20 nM. (C). Evaluation the effect of

steric hindrance of RCA products on the detection of miRNA let-7a based on RCA-FNA-LFA. (a) The result of agarose gel electrophoresis. Lane 1: D2000 marker. Lane 2: with nicking enzyme. Lane 3: without nicking enzyme. (b) miRNA let-7a detection based on RCA-FNA-LFA without nicking enzyme. Strip1: NC. Strip 2: 0.25 nM of miRNA let-7a detection. Strip 3: 0.5 nM of miRNA let-7a detection. Strip 4: 1 nM of miRNA let-7a detection. (c) miRNA let-7a detection based on RCA-FNA-LFA without nicking enzyme. Strip1: NC. Strip 2: 0.25 nM of miRNA let-7a detection. Strip 3: 0.5 nM of miRNA let-7a detection. Strip 4: 1 nM of miRNA let-7a detection

(RCA-FNA-LFA) was illustrated in Fig. 5, demonstrating a strategy for fast, simple, and visual detection of miRNA let-7a.

For miRNA detection, the padlock probe first specifically bound with miRNAs and cyclized in the presence of Splint R ligase. Once the padlock probe was cyclized, the amplification was started under the function of Phi29 DNA polymerase and repeated single-stranded amplified products were produced. The pre-prepared FNA nanomaterial combined with RCA product, and the formed complexes run along the NC membrane under the action of capillary force. Afterwards it was bound with the capture probe immobilized on the T line, and positive signal as red color was given. The strengthened red color indicated greater amount of RCA products on the T line. In contrast, in the absence of miRNA, that is, absence of RCA products, the FNA nanomaterial was not recognized by the capture probe immobilized on the T line, thereby negative signal (no red color) was given. Whereas all control reactions gave positive signals on the C line of the strip. The process of nanoscaffold self-assembly

was independent of the target sequence, so it is prepared in advance, and the entire detection process is only determined by the time of RCA amplification. Hence, the detection time was 2 h.

Considering the environmental factors and matrix factors that may affect the color rendering conditions, the color rendering ratio of T/C was used in the following results to counteract the inherent heterogeneity of LFA.

#### Optimization of RCA conditions for the proposed RCA-FNA-LFA assay

The specificity of the designed padlock probe was significant to ensure the specificity of the proposed method for target miRNA. Using pre-designed padlock probe LP let-7a, RCA was performed with the presence of miRNA 21, miRNA 221, and miRNA let-7a, respectively, and the results were characterized by agarose gel electrophoresis. A highly efficient RCA reaction would occur with a long repeating sequence that can be formed with low mobility



on agarose gel electrophoresis and signal can be identified on the gel lane. As shown in Fig. 6A, only Lane 2 with the presence of miRNA let-7a had obvious bright band near gel lane, indicating the designed padlock probe possessed a good specificity for miRNA let-7a.

RCA products and padlock probes had the homologous complementary sequences. Hence, excessive padlock probes in the system might prevent the binding of the RCA amplified products with the capture probes on T line of LFA. However, a lower concentration of padlock probe cannot efficiently perform RCA. Therefore, it was necessary to optimize the concentration of padlock probes. A gradient concentration of padlock probe (1, 5, 10, 50, and 100 nM) was used to evaluate the effect of padlock probe concentration on RCA reaction. As shown in Fig. 6B(a), bright bands appeared in Lane 3 (10 nM), Lane 4 (50 nM), and Lane 5 (100 nM), indicating that a large number of RCA products were produced with the concentration of padlock probes higher than 10 nM. All the above-mentioned RCA products were detected by the proposed RCA-FNA-LFA. According to the results in Fig. 6B(b), it can be found that an obvious signal appeared on the T line at the padlock probe concentration of 5 nM. With the padlock probe concentration increasing from 5 to 50 nM, the red color on T line became more clearer, while the color became weaker at padlock probe concentration of 100 nM, suggesting that 100 nM padlock probe might be excess and affect the detection process. Therefore, 50 nM was selected as the optimal concentration for padlock probe.

The product of RCA was a repeated long fragment, as well as the sequence length of the prepared FNA was generally above 2 Kb. Therefore, the complex of RCA-FNA may be too huge to affect its smooth migration on LFA. In order to overcome this possible influence, a nicking enzyme site was deliberately introduced into padlock probe to produce small fragments for smooth migration of the complex on LFA. With the addition of nicking enzyme, the product was changed from the accumulation on the gel lane to a diffuse band [Fig. 6C(a)]. It was worth noting that the efficiency of one-pot (Lane 2) digestion was higher than that of step-by-step (Lane 3). Subsequently, the RCA-FNA complex before and after digestion was also characterized with LFA (Fig. 6C). Compared with the undigested group [Fig. 6C(b)], the signal on T line was more obvious under the function of nicking enzyme [Fig. 6C(c)]. The smaller molecular weight of the complexes produced after enzyme digestion was easier to migrate on LFA, moreover, the exposed recognition sequence after digestion was more easily to be captured by the immobilized probe on T line.

### Optimization of running buffer for the proposed RCA-FNA-LFA assay

The composition of the running buffer had a great influence on the migration and capture of the RCA-FNA complex. For running buffer evaluation, the running buffer type, the running buffer pH values, type and percentage of detergent were the subjects of frequent inspection.

Three types of buffers (PBS, SSC, and Tris-HCl) were chosen to evaluate the efficiency for running buffer. Moreover, referring to previous studies, different concentrations of SSC (1×, 5×, and 10×) were also investigated due to their different function in nucleic acid hybridization [33, 34]. All the strips showed clear T line and C line in the presence of different running buffers (Fig. 7A), however, among the results of these running buffers, the T/C ratio in the 5×SSC buffer was the highest, thus it was chosen as the optimal running buffer for the detection.

Not AuNPs were easily to be destroyed but nucleic acid hybridization would fail under the condition of over-acid or over-alkali. Hence, the effect of pH values from 4 to 9 of 5×SSC running buffer were also evaluated (Fig. 7B). It was an obvious false positive phenomenon at acid condition (pH 4–6). From the results of three other pH values (pH 7–9), it was observed that the T/C ratio of 5×SSC buffer with pH value of 8 was the highest. There might be two main reasons for the effect of pH on the signal output of LFA. On one hand, nucleic acid molecules (DNA and RNA) had negatively charged phosphate groups, whose charge state was affected by pH. At different pH values, the degree of dissociation of nucleic acid molecules was different, affecting the ability to bind with the complementary chains [35]. On the other hand, pH had an effect on the stability of nucleic acid immobilization. For example, when the solution was alkaline, the positive charge on the of paper surface was reduced, which was not conducive for DNA immobilization. It meant lower the efficiency of DNA immobilization [36]. Therefore, 5×SSC with pH value of 8 was selected as the running buffer in the subsequent experiments.

The absence of surfactants in running buffer may result in low fluidity of RCA-FNA complexes and incomplete migration along NC membranes. First, two surfactants (Tween-20 and Triton X-100) with the same concentration (1%) were compared. As shown in Fig. 7C(a), running buffer added 1% Tween-20 showed a more obvious signal on T line than that of Triton X, however, Tween-20 as surfactant was accompanied by distinct false positive. In this study, Tween-20 may change the physical and chemical properties of the sample pad and the nitrocellulose membrane on the strip, or produces unexpected interactions with HCR nanoscaffolds-based functional nucleic acids on the strip, resulting in the generation of false positive signals. Another possible reason is that the presence of Tween-20 may alter the bonding

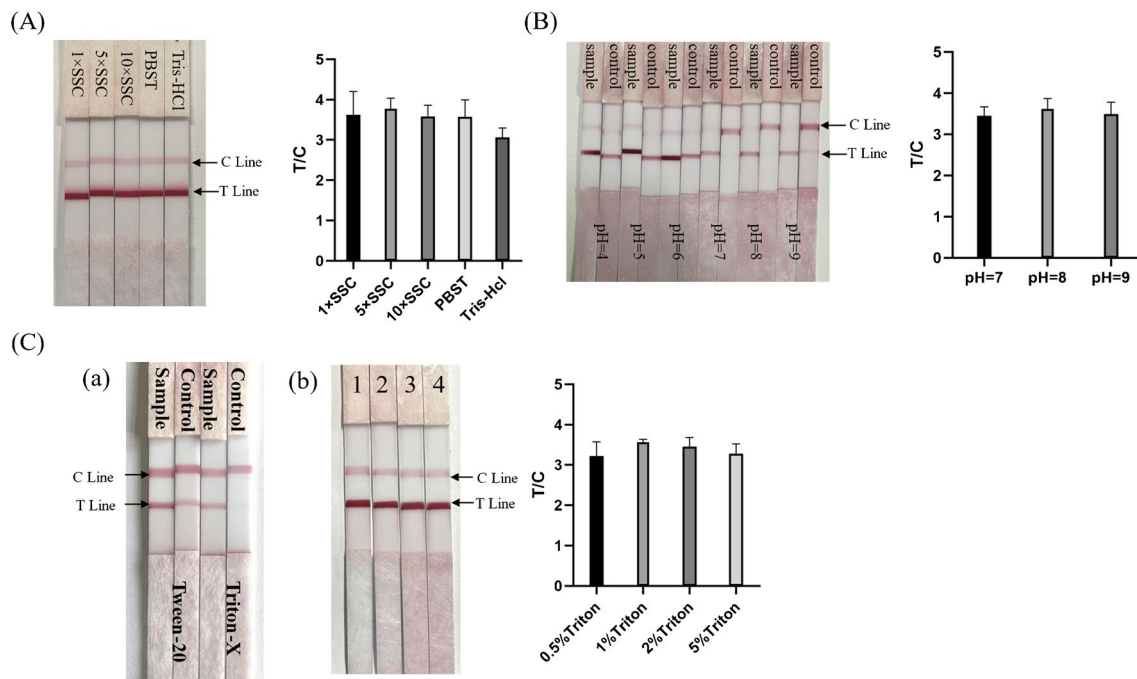


**Fig. 7** Optimization of detection conditions for the proposed RCA-FNA-LFA assay **(A)**. Optimization of running buffer types. **(B)**. Optimization of 5xSSC running buffer pH values. **(C)**. Optimization of

surfactant type and concentration. **(a)** Optimization of surfactant type. **(b)** Optimization of surfactant Triton X-100 concentration

dynamics between target miRNA-FNA complex and capturing probe on the strip [37, 38]. Thus, Triton X was chosen as the surfactant. Different concentrations of Triton X-100 (0.5%, 1.0%, 2.0%, and 5.0%, v/v) were further evaluated for their effect on LFA (Fig. 7C(b)). It can be found that when the concentration of Triton X-100 was 1.0%, the T/C ratio was the highest. Therefore, 1.0% Triton X-100 was finally selected as the surfactant in the subsequent experiments.

### Analytical performance of the proposed RCA-FNA-LFA assay

#### Sensitivity of the proposed RCA-FNA-LFA assay

Under the optimized experimental conditions, a gradient concentration of miRNA let-7a (0 nM, 25 pM, 50 pM, 100 pM, 250 pM, 500 pM, and 1 nM) were detected by the proposed RCA-FNA-LFA assay. As shown in Fig. 8, all concentrations of miRNA let-7a showed positive signals (red color) on T line, whereas absence of miRNA didn't give any positive signal (no red) on T line. With the increase of miRNA let-7a concentration, the red color of T line was strengthened, that is, the intensity of positive signal (red color) was proportional to the concentration of miRNA let-7a. The T/C ratio was linearly correlated with the logarithmic concentrations of miRNA let-7a with the linear regression of  $y = 0.35x - 0.5332$  ( $R^2 = 0.9561$ )

(Fig. 8B). The limit of detection (LOD) for miRNA let-7a was calculated to be 1.07 pM according to  $3\sigma$  principle, which was nearly 20-fold sensitivity enhancement compared with that of RCA-LFA assay [39].

Compared to other miRNA detection strategy, it can be observed that the sensitivity assay of the present study was slightly better than that of previous reported studies (Table 2).

#### Specificity of the proposed RCA-FNA-LFA assay

In order to evaluate the specificity of the proposed RCA-FNA-LFA assay, miRNA let-7 family members (let-7b, let-7c, let-7f, miR-202, and miR98) and other miRNAs (miR21 and miR133) were detected as the targets. 500 pM of different miRNAs and miRNA mixture were dissolved in fetal bovine serum (FBS) for detection. As illustrated in Fig. 9, for let-7a and miRNA mixture detection, obvious red bands on the T and C line were observed, while no bands were observed on T line of other miRNA groups. Meanwhile, the T/C ratio of let-7a and miRNA mixture group was significantly different from that of other groups. Hence, the present assay can be used for specific, sensitive, rapid, and visual detection of let-7a in serum samples, other miRNAs did not cause any interference to the detection.

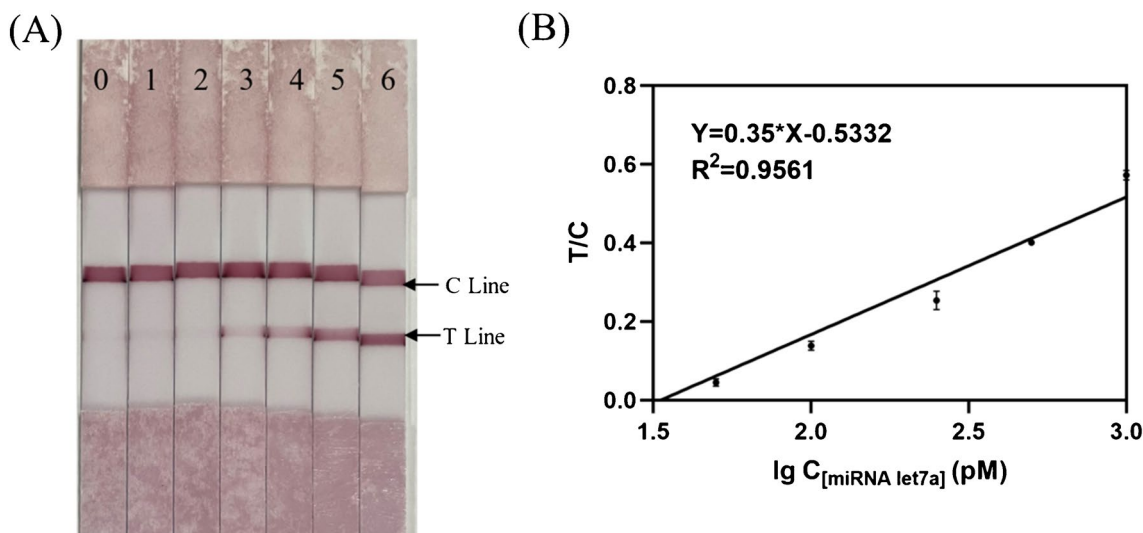


**Fig. 8** Sensitivity of the proposed RCA-FNA-LFA assay (A). Results of different miRNA let-7a concentrations detection by RCA-FNA-LFA. 0: negative control. 1–6 miRNA let-7a concentration: 25 pM,

50 pM, 100 nM, 250 nM, 500 pM, 1 nM, respectively. (B). Quantitative standard curve of miRNA let-7a detection. All values are mean  $\pm$  standard deviation ( $n=3$ )

**Table 2** Comparison of the results for miRNA detection

Target	Signal amplification method	LOD	Time	Reference
miRNA-21	RCA	40 pM	2 h	[39]
miRNA let-7a		20 pM		
miRNA-21	DSN enzyme	0.16 pM	2 h	[40]
miRNA-21	CHA	0.89 pM	1 h	[41]
miRNA-196a-5p	CHA	1.171 nM	30 min	[42]
miRNA-31-5p		2.251 nM		
miRNA-21	CHA	3.31 pM	30 min	[43]
miRNA-196a-5p		2.18 pM		
miRNA let-7a	RCA-FNA	1.07 pM	2 h	This work

**Accuracy of the proposed RCA-FNA-LFA assay**

The accuracy and precision of the proposed RCA-FNA-LFA assay were evaluated by detecting miRNA let-7a spiked in FBS, and the recovery was calculated. Low (100 pM), medium (250 pM), and high concentrations (1 nM) of miRNA let-7a were spiked in FBS for analysis. As shown in Table 3, the intra-assay recoveries were  $96.64 \pm 2.05\%$ ,  $99.41 \pm 2.15\%$ , and  $100.10 \pm 0.81\%$ , and the inter-assay recoveries were  $97.25 \pm 9.08\%$ ,  $99.57 \pm 5.15\%$ , and  $100.57 \pm 1.80\%$ , respectively. The coefficient of variation was from 2.06 to 9.34%. These results indicated that the accuracy and precision of RCA-FNA-LFA was acceptable for the quantitative detection of miRNA let-7a.

**Stability of the proposed RCA-FNA-LFA assay**

To evaluate the stability, the HCR-based FNA nanomaterials in the solution or embedded on the conjunction pad were placed at 4°C and 37 °C for 7 days (equivalent to 1–2.5 months at low temperature), respectively. At each day post the incubation, the LFA were used to test 500 ng/mL miRNA let-7a. As shown in Fig. 10, there was no significant difference between three groups within 7 days, and the ratio of T/C value were all nearly 0.4. The results indicated that the proposed RCA-FNA-LFA assay was stable, and the prepared HCR-based FNA nanomaterials could be stably stored as well.

**Conclusions**

A novel functional nucleic acid nanomaterial based on HCR nanoscaffolds was proposed to solve the problems of time superposition and repeated primer design in cascaded amplification in the present study. The key factors that affect the self-assembly of FNA nanomaterials, such as assembly time, probe concentration, and system composition were focused to be investigated. Subsequently, using miRNA let-7a as the model target, RCA was cascaded with FNA nanomaterials and LFA for sensitive and rapid detection. Under the optimal conditions, the proposed RCA-FNA-LFA assay demonstrated the specificity and accuracy of miRNA let-7a detection with a detection limit of 1.07 pM and a detection range of 25–1000 pM, which was nearly 20-fold sensitivity enhancement compared with that of RCA-LFA assay. It

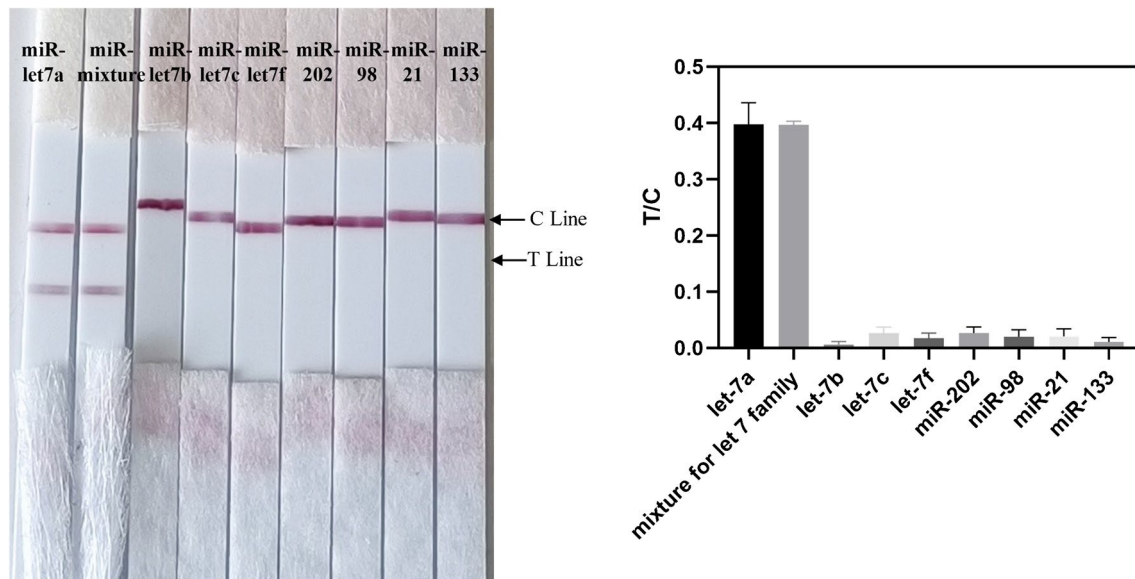


**Fig. 9** Specificity of the proposed RCA-FNA-LFA assay

**Table 3** The accuracy and precision of RCA-FNA-LFA for detection of miRNA let-7a spiked in serum

miRNA let-7a (pM)	Intra-assay				Inter-assay			
	Mean (pM)	SD	Recovery (%)	CV (%)	Mean (pM)	SD	Recovery(%)	CV (%)
100	99.64	2.05	96.64 ± 2.05%	2.06	97.25	9.08	97.25 ± 9.08%	9.34
250	248.52	5.38	99.41 ± 2.15%	2.16	248.93	12.87	99.57 ± 5.15%	5.17
1000	1001.03	8.01	100.10 ± 0.81%	0.80	1005.72	18.02	100.57 ± 1.80%	1.79

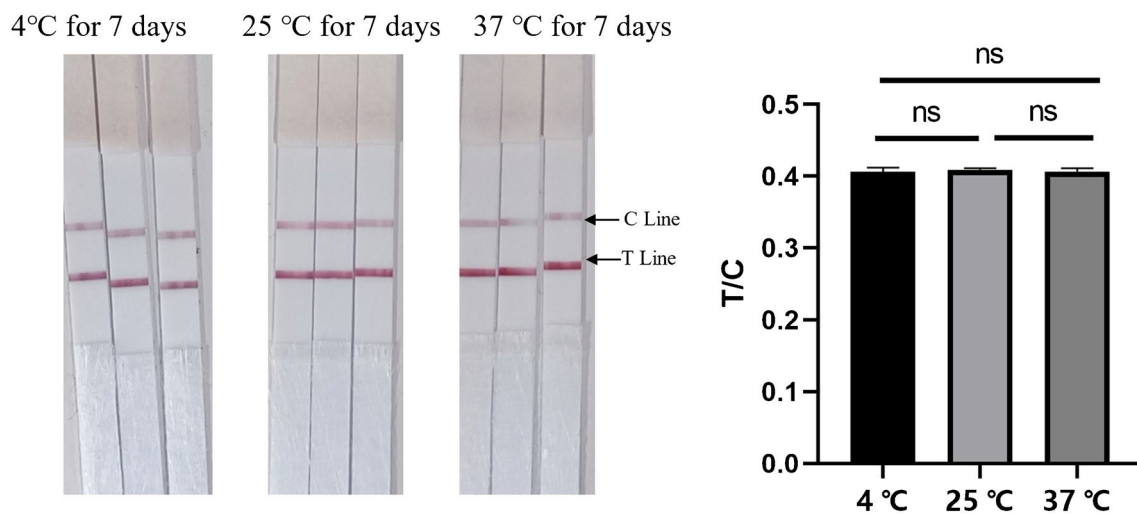


**Fig. 10** The stability of HCR-based FNA nanomaterials

was worth mentioning that the time consumption of the proposed cascaded amplification based on RCA-FNA-LFA in this study only depended on the time of RCA, because FNA nanomaterials were prepared in advance. At the same time,

a standardized FNA probe design was established, which depended on the design of padlock probes for RCA. As for other targets detection, the developed FNA nanomaterials can be used without any change. It can be expected that

this smart design will play a pivotal role in greatly reducing duplication of effort in probe design. Meanwhile, by combining with labels with stronger signal intensity, such as fluorescence and surfaced enhanced Raman spectroscopy (SERS), the sensitivity of the proposed assay can be significantly enhanced and realizes ultra-sensitive detection.

**Acknowledgements** This work was financially supported by National Key Research and Development Program of China (2022YFC2602900-03).

**Data availability** Data and materials will be made available on request.

## Declarations

**Ethical approval** This article does not contain any study with human participants or animals performed by any of the authors.

**Conflict of interest** The authors declare no competing interests.

## References

- Islam MM, Koirala D (2022) Toward a next-generation diagnostic tool: A review on emerging isothermal nucleic acid amplification techniques for the detection of SARS-CoV-2 and other infectious viruses. *Anal Chim Acta* 1209:30
- Glökler J, Lim TS, Ida J, Frohme M (2021) Isothermal amplifications - a comprehensive review on current methods. *Crit Rev Biochem Mol* 56:543–586
- Nieuwkerk DM, Korajkic A, Valdespino EL, Herrmann MP, Harwood VJ (2020) Critical review of methods for isothermal amplification of nucleic acids for environmental analysis. *J Microbiol Meth* 179:11
- Du MY, Mao GB, Tian SB, Liu YC, Zheng J, Ke XL, Zheng ZH, Wang HZ, Ji XH, He ZK (2019) Target-Induced Cascade Amplification for Homogeneous Virus Detection. *Anal Chem* 91:15099–15106
- Sun HH, He F, Wang T, Yin BC, Ye BC (2020) A Cas12a-mediated cascade amplification method for microRNA detection. *Analyst* 145:5547–5552
- Jiang H, Li Y, Lv XF, Deng YL, Li XQ (2023) Recent advances in cascade isothermal amplification techniques for ultra-sensitive nucleic acid detection. *Talanta* 260:18
- Luo ZW, Li YX, Zhang P, He L, Feng YT, Feng YQ, Qian C, Tian YH, Duan YX (2022) Catalytic hairpin assembly as cascade nucleic acid circuits for fluorescent biosensor: Design, evolution and application. *Trac-Trends Anal Chem* 151:27
- Reynolds J, Loeffler RS, Leigh PJ, Lopez HA, Yoon JY (2023) Recent Uses of Paper Microfluidics in Isothermal Nucleic Acid Amplification Tests. *Biosensors-Basel* 13:28
- Hu XX, Zhang H, Zhou Y, Liang WB, Yuan R, Chen SH (2019) A fluorometric lead(II) assay by using a DNA dendrimer as a carrier for the immobilization of the signal probe. *Microchim Acta* 186:6
- Li T, Duan RL, Duan ZJ, Huang FJ, Xia F (2020) Fluorescence Signal Amplification Strategies Based on DNA Nanotechnology for miRNA Detection. *Chem Res Chinese U* 36:194–202
- Jiang H, Lv XF, Li Y, Deng YL, Yu SY (2023) A cascade amplification strategy based on rolling circle amplification and hybridization chain reaction for ultrasensitive detection of pathogens. *Anal Methods* 15:2382–2390
- Jia HY, Zhao HL, Wang T, Chen PR, Yin BC, Ye BC (2022) A programmable and sensitive CRISPR/Cas12a-based MicroRNA detection platform combined with hybridization chain reaction. *Biosens Bioelectron* 211:7
- Xu WT, He WC, Du ZH, Zhu LY, Huang KL, Lu Y, Luo YB (2021) Functional Nucleic Acid Nanomaterials: Development. *Prop App Angew Chem Int Edit* 60:6890–6918
- Zhang WX, Chen ZZ, Shi Y, Wang JQ, Zhang JJ (2023) Integration of CRISPR/Cas with functional nucleic acids as versatile toolbox for non-nucleic acid target diagnostics: a review. *Flex Print Electron* 8:14
- Wang XX, Zhu LJ, Li ST, Zhang YZ, Liu SY, Huang KL, Xu WT (2021) Fluorescent functional nucleic acid: Principles, properties and applications in bioanalyzing. *Trac-trend Anal Chem* 141:34
- Zhang YZ, Zhu LJ, Tian JJ, Zhu LY, Ma X, He XY, Huang KL, Ren FZ, Xu WT (2021) Smart and Functionalized Development of Nucleic Acid-Based Hydrogels: Assembly Strategies, Recent Advances, and Challenges. *Adv Sci* 8:28
- Chaudhary P, Sharma R, Rawat S, Janmeda P (2023) Nucleic Acid Nanotechnology: Trends, Opportunities and Challenges. *Curr Pharm Biotechnol* 24:23–49
- Wang F, Li P, Chu HC, Lo PK (2022) Nucleic Acids and Their Analogues for Biomedical Applications. *Biosensors-Basel* 12:35
- Xu H, Zhang YF, Zhang SX, Sun MZ, Li WH, Jiang YF, Wu ZS (2019) Ultrasensitive assay based on a combined cascade amplification by nicking-mediated rolling circle amplification and symmetric strand-displacement amplification. *Anal Chim Acta* 1047:172–178
- Zhang Z, Zhang L, Wang YQ, Yao J, Wang T, Weng Z, Yang L, Xie GM (2021) Ultrasensitive electrochemical biosensor for attomolar level detection of let 7a based on toehold mediated strand displacement reaction circuits and molecular beacon mediated circular strand displacement polymerization. *Anal Chim Acta* 1147:108–115
- Niu C, Lin XJ, Jiang X, Guo F, Liu JX, Liu XQ, Huang HG, Huang Y (2022) An electrochemical aptasensor for highly sensitive detection of CEA based on exonuclease III and hybrid chain reaction dual signal amplification. *Bioelectrochemistry* 143:7
- Wei J, Xie X, Chang WD, Yang ZH, Liu YJ (2018) Ultrasensitive photoelectrochemical detection of microcystin-LR based on hybridization chain reaction assisted exciton-plasmon interaction and enzymatic biocatalytic precipitation. *Sens Actuator B-Chem* 276:180–188
- Zhou L, Wang Y, Yang C, Xu H, Luo J, Zhang WQ, Tang XQ, Yang S, Fu WL, Chang K, Chen M (2019) A label-free electrochemical biosensor for microRNAs detection based on DNA nanomaterial by coupling with Y-shaped DNA structure and non-linear hybridization chain reaction. *Biosens Bioelectron* 126:657–663
- Zhang X, Servos MR, Liu JW (2012) Instantaneous and Quantitative Functionalization of Gold Nanoparticles with Thiolated DNA Using a pH-Assisted and Surfactant-Free Route. *J Am Chem Soc* 134:7266–7269
- Zadeh JN, Steenberg CD, Bois JS, Wolfe BR, Pierce MB, Khan AR, Dirks RM, Pierce NA (2011) NUPACK: Analysis and Design of Nucleic Acid Systems. *J Comput Chem* 32:170–173
- Fornace ME, Porubsky NJ, Pierce NA (2020) A Unified Dynamic Programming Framework for the Analysis of Interacting Nucleic Acid Strands: Enhanced Models, Scalability, and Speed. *ACS Synth. Biol* 9:2665–2678
- Sun H, Yao FJ, Su ZQ, Kang XF (2020) Hybridization chain reaction (HCR) for amplifying nanopore signals. *Biosens Bioelectron* 150:7
- Wu MS, Xu N, Qiao JT, Chen JH, Jin LS (2019) Bipolar electrode-electrochemiluminescence (ECL) biosensor based on a hybridization chain reaction. *Analyst* 144:4633–4638

29. Wang J, Shimada N, Maruyama A (2022) Cationic Copolymer-Augmented DNA Hybridization Chain Reaction. *ACS Appl Mater Interfaces* 14:39396–39403
30. Li F, Yu WT, Zhang JJ, Dong YH, Ding XH, Ruan XH, Gu Z, Yang DY (2021) Spatiotemporally programmable cascade hybridization of hairpin DNA in polymeric nanoframework for precise siRNA delivery. *Nat Commun* 12:12
31. Wu Q, Yang L, Xie LL, Shang JH, He SZ, Liu J, Wang F (2022) Modular Assembly of a Concatenated DNA Circuit for In Vivo Amplified Aptasensing. *Small* 18:12
32. Wang JB, Chao J, Liu HJ, Su S, Wang LH, Huang W, Willner I, Fan CH (2017) Clamped Hybridization Chain Reactions for the Self-Assembly of Patterned DNA Hydrogels. *Angew Chem Int Edit* 56:2171–2175
33. Baka EC, Kalogianni DP (2022) A signal-enhanced DNA-based lateral flow assay. *Microchem J* 183:6
34. Jauset-Rubio M, El-Shahawi MS, Bashammakh AS, Alyoubi AO, O'Sullivan CK (2017) Advances in aptamers-based lateral flow assays. *Trac-Trends Anal. Chem* 97:385–398
35. Qu ZB, Zhang YA, Dai ZZ, Hao YY, Zhang YC, Shen JL, Wang F, Li Q, Fan CH, Liu XG (2021) DNA Framework-Engineered Long-Range Electrostatic Interactions for DNA Hybridization Reactions. *Angew Chem-Int Edit* 60:16693–16699
36. Zhou W, Feng ML, Valadez A, Li XJ (2020) One-Step Surface Modification to Graft DNA Codes on Paper: The Method, Mechanism, and Its Application. *Anal Chem* 92:7045–7053
37. Sakurai A, Takayama K, Nomura N, Yamamoto N, Sakurai Y, Kobayashi Y, Kida H, Shibasaki F (2014) Multi-colored immunochromatography using nanobeads for rapid and sensitive typing of seasonal influenza viruses. *J Virol Methods* 209:62–68
38. Eryilmaz M, Soykut EA, Çetin D, Boyacı IH, Suludere Z, Tamer U (2019) SERS-based rapid assay for sensitive detection of Group A *Streptococcus* by evaluation of the swab sampling technique. *Analyst* 144:3573–3580
39. Yao MD, Lv XF, Deng YL, Rasheed M (2019) Specific and simultaneous detection of micro RNA 21 and let-7a by rolling circle amplification combined with lateral flow strip. *Anal Chim Acta* 1055:115–125
40. Wei HJ, Peng YJ, Bai ZK, Rong Z, Wang SQ (2021) Duplex-specific nuclease signal amplification-based fluorescent lateral flow assay for the point-of-care detection of microRNAs. *Analyst* 146:558–564
41. Wang WJ, Li Y, Nie AX, Fan GC, Han HY (2021) A portable SERS reader coupled with catalytic hairpin assembly for sensitive microRNA-21 lateral flow sensing. *Analyst* 146:848–854
42. Cao XW, Sun Y, Mao Y, Ran ML, Liu YF, Lu D, Bi CL (2021) Rapid and sensitive detection of dual lung cancer-associated miRNA biomarkers by a novel SERS-LFA strip coupling with catalytic hairpin assembly signal amplification. *J Mater Chem C* 9:3661–3671
43. Mao Y, Sun Y, Xue J, Lu WB, Cao XW (2021) Ultra-sensitive and high efficiency detection of multiple non-small cell lung cancer-related miRNAs on a single test line in catalytic hairpin assembly-based SERS-LFA strip. *Anal Chim Acta* 1178:14

**Publisher's Note** Springer Nature remains neutral with regard to jurisdictional claims in published maps and institutional affiliations.

Springer Nature or its licensor (e.g. a society or other partner) holds exclusive rights to this article under a publishing agreement with the author(s) or other rightsholder(s); author self-archiving of the accepted manuscript version of this article is solely governed by the terms of such publishing agreement and applicable law.